INTERNATIONAL JOURNAL OF CLIMATOLOGY
Int. J. Climatol. **31**: 289–301 (2011)
Published online 27 October 2010 in Wiley Online Library
(wileyonlinelibrary.com) DOI: 10.1002/joc.2240

RMetS
Royal Meteorological Society

Representing complex urban geometries in mesoscale modeling

Adil Rasheed,[a]* Darren Robinson,[b] Alain Clappier,[c] Chidambaram Narayanan[d] and Djamel Lakehal[d]

[a] *Research Scientist, SINTEF ICT, Department of Applied Mathematics, Alfred Getz vei 1, Trondheim, Norway*
[b] *Senior Scientist, EPFL-ENAC-ICARE-LESO-PB, Station 18, CH-1015 Lausanne, Switzerland*
[c] *Université de Strasbourg, Laboratoire Image Ville Environnement, CNRS, labo n° ERL 7230, 3, Rue de l'Argonne, 67000 Strausborg, France*
[d] *CEO ASCOMP GmbH, Technoparkstr. 1, Newton, CH-8005 Zurich, Switzerland*

ABSTRACT: Real cities are comprised of a diverse, random arrangement of building positions, shapes, and sizes. Yet most of the urban parameterisations thus far developed share the assumption that a city is made up of either a regular array of parallelepipeds or infinitely long canopies. The inputs to these models, which include street width, building width, building density and a statistical representation of building heights, are generally obtained through quantitative field surveys (which are very slow and time consuming to perform) or qualitative estimates from Digital Elevation Model. But in performing this geometric abstraction there is no way to ensure that the total built surfaces and volumes of the simplified geometry match those of the actual city, or more importantly, that the energy and momentum exchanges are equivalent. In this paper, we aim to test the central hypothesis that cities can be accurately represented by a regular array of parallelepipeds or canopies. For this, we investigate, for a particular scenario, the effects of complexity in urban geometry on the spatially averaged drag forces and shortwave radiation exchange. For drag computation, we used the Immersed Surface Technique, while for computing the incident radiation we used the Simplified Radiosity Algorithm. After testing the above hypothesis, we propose a new approach for fitting an array of cubes to any complex (realistic) geometry, so that new or existing urban parameterisation schemes can be used with confidence. Copyright © 2010 Royal Meteorological Society

KEY WORDS mesoscale modeling; urban canopy model; complex urban geometry

Received 15 October 2009; Revised 13 September 2010; Accepted 13 September 2010

1. Introduction

The local climate of a city has a direct impact on buildings' energy demand for heating or cooling. This impact can be exacerbated, or otherwise, by the Urban Heat Island effect whose existence has been scientifically established through field experiments and numerical studies. The Urban Heat Island is a phenomenon where an urban area/city experiences on average, higher temperatures than the surrounding rural areas due to increased net radiation and absorption of heat by urban surfaces which have very different thermophysical properties compared to rural surfaces. Since its impacts on energy demand and comfort is highly non-linear, there is a need for tools which can estimate this impact in a physically realistic and accurate way. This is where various geophysical codes/software based on the basic principles of fluid dynamics come into play. However, all these tools have a common shortfall associated with the diverse spatio-temporal scales involved with urban climate modeling. The climate in a city, for example, will be affected not only by the buildings and urban canopies (size of a few meters) but also by large topographical features such as oceans, lakes, and mountains (the size of a few kilometers). Unfortunately, it is not possible to satisfactorily resolve all these scales in a computationally tractable way using a single model. Generally, the scales bigger than those that a model can handle are referred to as super scales, and those at smaller scales are referred to as sub-grid scales. In urban climate modeling, it is quite the norm now to include the effects of the former using appropriate forcing at the boundaries, and the latter by using parameterisations. A group of buildings forming urban canopies can affect the local climate in two important ways: firstly, by retarding the air flow in their vicinity which is a direct consequence of the drag and shear forces that they offer owing to their complex shapes, and secondly, by modifying the energy balance associated with the net absorption of radiation (both shortwave and longwave) due to sun and sky occlusions and inter-reflections between occluding surfaces. Surfaces' thermophysical properties can also have a significant impact on retarding surface-air heat transfer. These surfaces can also affect turbulence production due to the formation of wake vortices. A detailed review of the effects of urban texture on the flow characteristics, shear-stress profile,

* Correspondence to: Adil Rasheed, Research Scientist, SINTEF ICT, Department of Applied Mathematics, Alfred Getz vei 1, Trondheim, Norway. E-mail: adil.rasheed@sintef.no

mean-velocity profile, turbulence intensities and dispersion characteristics can be found in the work by Britter and Hanna (2003). A way of modeling these effects is to couple an Urban Canopy Model (UCM) with a Building Energy Model (BEM). Many such couplings exist, as will be described in the next section. However, most of them assume a city to be comprised of a regular array of parallelepipeds. In this paper, we investigate the importance of this assumption and go on to suggest a procedure for mapping real complex urban geometries onto simplified equivalents that are compatible with existing UCMs to improve the predictive accuracy of urban climate models.

2. Background

In order to more accurately model the physics of an urban canopy, new concepts in surface modeling have been developed. These models aim to solve the surface energy balance (SEB) for a realistic 3-D urban canopy. Almost all of them share the following characteristics in their constructions: (1) 3-D shapes of the buildings and their impacts on drag and shear forces are represented; (2) A distinction is made between roof, street, and wall surfaces; (3) Radiative interactions between streets and walls are accounted for, albeit in a crude way; and (4) Cities are represented by a regular array of parallelepipeds.

These models consist of horizontal and vertical representations of urban structures. The vertical surfaces represent building walls, and horizontal surfaces represent streets and roofs. Since a clear distinction between these surfaces is made, it is convenient to assign different values of thermo-physical parameters to them and to model them differently. Such simple models use a highly simplified approach to compute complex radiation exchanges, as in the work by Noihan (1981) which is based on view factors between different surfaces or facets comprising those surfaces. Solar reflections and occlusion to the sun and the (normally isotropic) sky are also explicitly resolved. Surface temperatures, energy exchanges with the surroundings, and energy storage in the built material are computed by solving a set of 1-D conduction equation for different types of surfaces. These models can be separated into two main categories: those where the canopy air is parameterised, as in Masson (2000) town energy balance (TEB), and those that use a drag approach, as for forests, but here, with buildings (Martilli *et al*. 2002). Here, the first type is referred to as a single-layer model because there is a direct interaction with only one atmospheric layer above the uppermost roof level. The second category is called multilayer model because several air layers are explicitly influenced by the buildings between the ground surface and the lowest atmospheric layer.

2.1. Single-layer models

In these models, exchanges between the surfaces and atmosphere occur only at the top of the canopies and roofs. This results in simplicity and computational efficiency, but since no equation is solved to compute the velocity, humidity, and temperature profiles inside the canopies, some assumptions are to be made. Generally, a logarithmic law for wind is assumed to apply down to the buildings' roof level, and an exponential decay law is used below (Swaid, 1993). Some models even use a constant velocity profile inside the canopy. Air humidity and temperature is assumed to be uniform inside the canopy. The simplest of these models is the TEB by Masson (2000) which makes use of just one generic roof, wall, and street. Other models falling into this category include those by Mills (1997) which consists of building blocks with streets intersecting each other at right angles, and Kusaka *et al*. (2001) which is similar to TEB, using canyon geometry, but with several canyons treated separately. Despite the many arguments (principally revolving around computational efficiency) in favor of single-layer models, the basic underlying assumption that the temperature, humidity, and wind velocity can be represented by a single value inside the canopy seems unreasonable (as will be shown later).

2.2. Multi-layer models

In these models, velocity, temperature, and humidity profiles are computed on a vertical grid. The vertical resolution opens up the possibility of treating the roofs, walls, and ground surfaces independently. Distinction can even be made between different points (depending upon the resolution) on the same vertical surfaces. These models thus allow for a more detailed and accurate treatment of multi-storied buildings (Salamanca *et al*., 2009). Among these models, that of Martilli *et al*. (2002) models the effects of street orientation and variations in building heights. This model, tested against wind turbulence data from Rotach (2001) and Roth (2000), is able to represent the differential heating of the wall surfaces due to the shading effects of local obstructions. Two other models of this type have been developed, one by Vu *et al*. (1999) and another by Kondo and Liu (1998). They are based on similar principles except that only one surface energy balance per wall is possible (there is no vertical resolution). In the model by Vu *et al*. (1999), the volume occupied by the buildings is more accurately taken into account. However, this comes at the cost of significant modifications to the atmospheric model equations. Mathematically, most multilayer canopy models are represented by the following set of equations:

$$\frac{\partial u}{\partial t} = \frac{\partial}{\partial z}\left(K_{zm}\frac{\partial u}{\partial z}\right) + Q_u \tag{1}$$

$$\frac{\partial v}{\partial t} = \frac{\partial}{\partial z}\left(K_{zm}\frac{\partial v}{\partial z}\right) + Q_v \tag{2}$$

$$\frac{\partial \theta}{\partial t} = \frac{\partial}{\partial z}\left(K_{z\theta}\frac{\partial \theta}{\partial z}\right) + Q_\theta \tag{3}$$

Here u and v are the horizontal velocity components, θ is the potential temperature, z is the vertical coordinate, and t is time. The basic assumption here is that a city

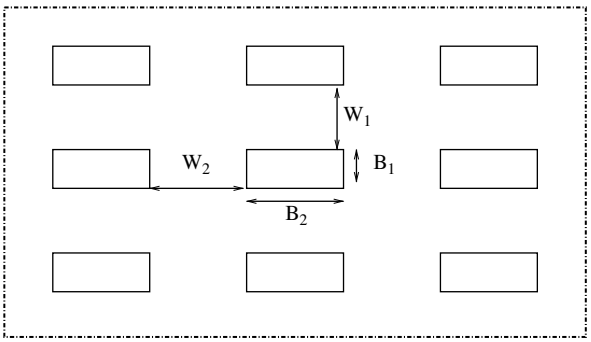

Figure 1. Regular array of parallelepipeds in an aligned configuration.

is represented by a regular array of parallelepipeds, as shown in Figure 1. The terms K_{zm}, $K_{z\theta}$ are turbulent coefficients for momentum and heat, while Q_u, Q_v, Q_θ represent the sources/sinks of the momentum and energy equations. These terms are parameterised in terms of the geometric parameters B_1, B_2, W_1, W_2 and street orientation. The term Q_θ also represents energy exchange with the buildings. It depends on the surface temperatures of the wall, ground, and roof. The thermo-physical properties of the materials constituting these three different types of surfaces are generally quite different and hence a differential heating of these surfaces (roof, wall, and ground) may lead to very different source terms. This differential heating can be caused by differences in incident irradiation and the canopy velocities which in turn will be affected by drag and shear forces.

3. Testing the hypothesis

Most of the canopy models need, as inputs, the street width and orientation, building width, building density, and a statistical representation of building heights which are generally obtained through quantitative field survey (which are very slow and time consuming to perform) or qualitative estimates. But in performing this geometric abstraction there is no way to ensure that the total built surfaces and volumes of the simplified geometry match those of the actual city, or more importantly, that the energy and momentum exchanges are equivalent. In this section we aim to test the central hypothesis that cities can be accurately represented by a regular array of parellelepipeds. For this we investigate, for a particular scenario, the effects of complexity in urban geometry on the spatially averaged drag forces and shortwave radiation exchanges with different surfaces (roofs, ground, and walls). Although some excellent work has been conducted in the past to study radiation exchange in urban canopies (e.g. Harman *et al*., 2004), these studies have necessarily been confined to simplified geometries due to the difficulties encountered in deriving an analytical form for the models' view factors (sky–wall, wall–wall, sky–ground, wall–ground, ground–ground). Since part of our aim from the outset was to model radiation exchange in real complex urban settings, but in a computationally reasonably way, we use Robinson and Stone's (2005) Simplified Radiosity Algorithm (SRA) (Appendix A). Drag computations using traditional CFD codes in a complex scenario are also complicated by the time and complexities associated with unstructured 3-D mesh generation. Also, the solution algorithms associated with unstructured solvers are not as efficient as those of structured solvers; hence, we have used the Immersed Surface Technique (IST). This has all the benefits of a structured solver and is capable of simulating flow around complex geometries. This technique has been implemented in the TransAT (2010) (Transport Phemona Analysis Tool) code, as explained in Appendix B.

3.1. Test Set-up

For this study, we have chosen a part of the city of Basel, which has a dimension of 1000 m × 750 m. A good approximation of the real geometry was sketched assuming that all the buildings have a uniform height of 15 m (H15). Many of the buildings in this part of Basel, a very dense city, have been constructed to this maximum height, although they do not necessarily all have flat roofs. However, our objective in this paper is not to attempt to reproduce reality. Rather, it is to test whether a simplified abstract representation of urban geometry can be used to reproduce similar energy and momentum exchanges to its real (complex) counter part. For this, a simplification of the third dimension of our geometry should not undermine the relevance of our study. The total built vertical and horizontal surface areas are presented in Table I. Three simplified representations of this geometry are also considered in the present investigation. These we refer to as long canopies, simple cuboids 1, and simple cuboids 2. The long-canopies representation of the city consists of ten rows of terraced buildings, each with a dimension of 500 m × 30 m with an interspacing of 67 m, as shown in Figure 2. Simple cuboids 1 consists of 20 × 18 cuboids each with a dimension of 20 m × 20 m × 15 m, and aligned in a regular array with a spacing of 30 m in the stream-wise direction, and 20 m in the span-wise direction, as shown in Figure 2. Similarly, the simple cuboids 2 representation consists of 20 × 18 cuboids, each with a dimension of 26.7 m × 15 m × 15 m aligned in a regular array with a spacing of 23.3 m in the stream-wise direction, and 25 m in the span-wise direction, as shown in Figure 2. For clarity, we present in Table II some associated geometric quantities: the building plan area fraction (λ_p) and the building wall area fraction (λ_w).

Table I. Geometric characteristics of built surfaces in the domain of interest.

Horizontal built area (roofs)	144 000 m^2
Vertical built area (walls)	432 000 m^2
Horizontal built area (ground)	606 000 m^2
Building height	15 m
Total built volume	2 160 000 m^2

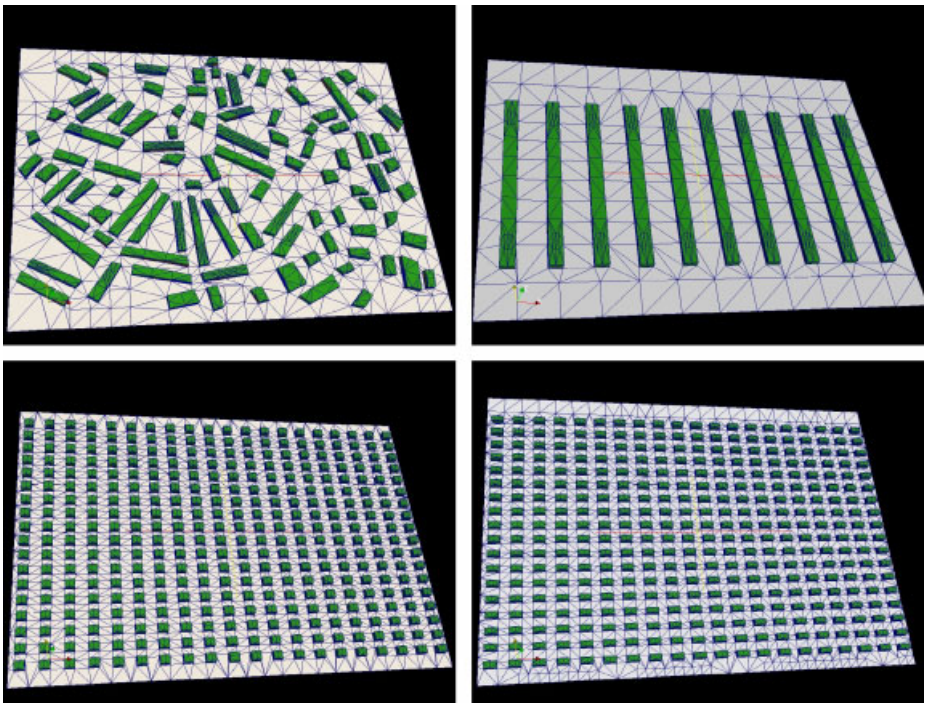

Figure 2. Four types of geometries under consideration: complex geometry (top left), long canopies (top right), simple cuboids 1 (bottom left) and simple cuboids (bottom right). This figure is available in colour online at wileyonlinelibrary.com/journal/joc

Here $\lambda_p = A_r/A_d$ and $\lambda_w = A_w/A_d$ where A_r is the total roof area, A_w is the total wall area and A_d is the total domain area. It should be noted that the building plan area fraction for all the representations under consideration are similar (approx 0.2). However, the wall area fraction for the long canopy is very different compared to the other representations. The intention here is to show that even when the built volume and roof area are conserved, the vertical wall area can differ significantly and have a severe impact on radiation exchange and air flow. In reality (from surveys) even basic quantities like the built volume are hardly conserved. Thus, by ensuring the equivalence of these quantities in our different representations, we focus on testing our underlying hypothesis that real geometries can be modeled with reasonable accuracy by their simplified representations.

3.2. Radiation analysis

As mentioned above, the magnitude of incident radiation varies with the type of surfaces (wall, roof, and ground) due to differences in surface tilt, orientation, and occlusion. This tends to result in different surface temperatures which in turn affect the quantity of energy being exchanged with the surroundings. To better understand this problem we investigate the differences in the amount of shortwave radiation incident on different surfaces for our simplified geometries of equivalent volume.

3.2.1. *Set-up for radiation computation*

For radiation computation, the surfaces in each of the representations are tessellated into smaller surfaces (Figure 2). The details of the tesselisation are shown in Table III. These simulations were conducted using the prevailing meteorological conditions on the 7th of January 2008.

3.2.2. *Radiation results*

All domains of the same size will have the same amount of solar radiation entering them. But as discussed already, for mesoscale modeling, a correct calculation of the distribution of radiation amongst the wall, roof, and ground surfaces is very important, as this determines the total absorption of radiation within the domain and the corresponding energy that is transferred to the adjacent air. Variations in the spatial distribution of absorbed

Table II. Roof area A_r, domain area A_d, wall area A_w, building plan area fraction L_p and wall area fraction L_w.

	A_r (m^2)	A_d (m^2)	A_w (m^2)	λ_p	λ_w
Long canopies	150 000	750 000	159 000	0.200	0.21
Simple cuboid 1	144 000	750 000	432 000	0.192	0.57
Simple cuboid 2	144 180	750 000	450 360	0.192	0.60
Real morphology	144 000	750 000	432 000	0.192	0.57

Table III. Number of triangles to discretise different surfaces.

Cases	Roofs	Ground	Walls
Complex	992	870	2658
Long canopies	420	284	400
Simple cuboids 1	2160	2242	7520
Simple cuboids 2	2160	2396	8640

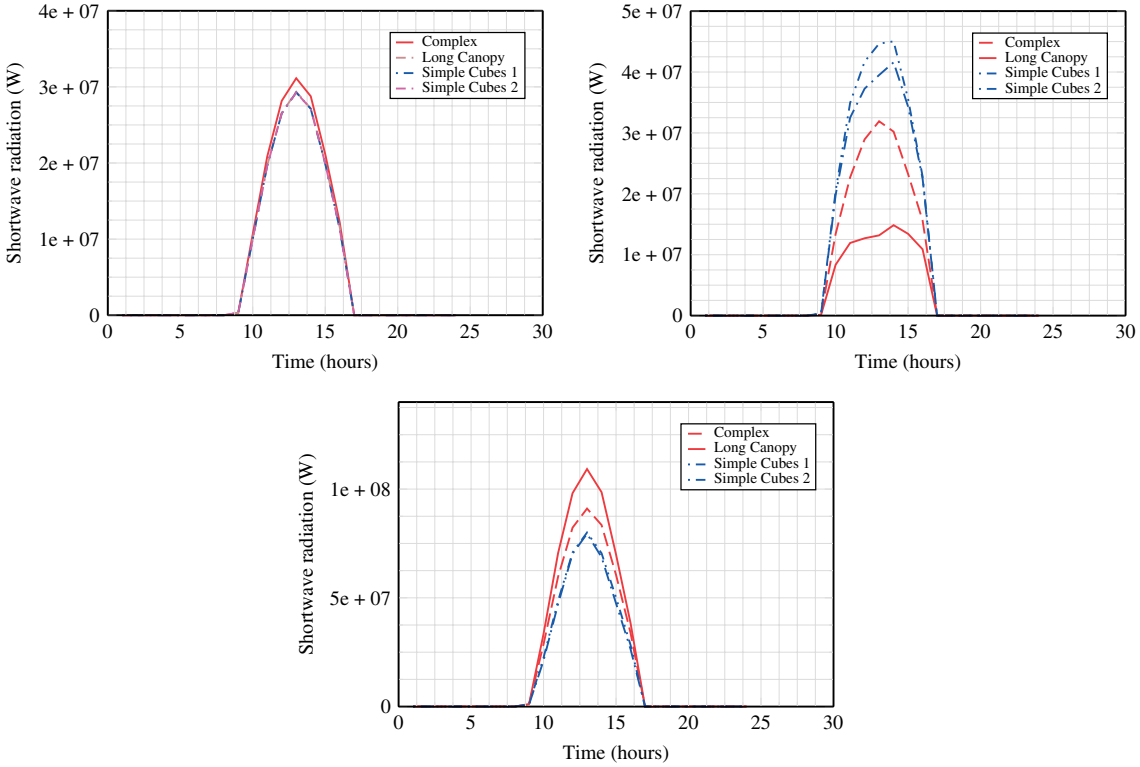

Figure 3. Hourly comparison of the amount of shortwave radiation incident on roof (top left), wall (top right) and ground (bottom) surfaces for the four representations. This figure is available in colour online at wileyonlinelibrary.com/journal/joc

solar energy may also modify momentum transfers. From Figure 3 we make the following observations: (1) Roofs: Since the horizontal roof surface areas in all four of our representations are the same, and all the buildings are of the same height (and hence there is no obstruction to the sky), we observe that the amount of radiation absorbed during the whole day is similar, as expected; (2) Ground: In the particular case of long canopies, the ground receives more solar radiation than either of the cuboid layouts, as views to the sun and sky are relatively unobstructed. In the complex representation, these views are relatively obstructed so that the radiation incident on the ground decreases. In the case of the two cuboid representations, views are even further obstructed, so that even less solar radiation is incident on the ground of our domain; (3) Walls: The two simplified cuboid representations receive more shortwave radiation than the complex and long-canopy representations. This is due to an increased reflected contribution and an increased south-facing surface area. Thus, for this particular day, the walls in the simplified representation will be warmer than in the complex one. The opposite will be true for the ground surfaces. This will result in different surface temperatures for the walls and ground with a corresponding influence on surface energy exchanges.

3.3. CFD analysis

3.3.1. Set-up for CFD simulations

To investigate the drag characteristics of the four configurations, we employed a CFD code called TransAT (TransAT, 2010). The code is a structured curvilinear grid-based Navier Stokes solver for incompressible and weakly compressible flows. To the authors' knowledge, this is the only commercial code available which supports the use of the Immersed Surface Technique for simulating urban flows, as described in Appendix B. Some validation results to prove the reliability of the method are also presented in the Appendix B.

For the present analysis, the geometrical representations are the same as those used for radiation calculations. However, the domain has been extended at all four boundaries by an additional distance of 13H resulting in a total distance of 15H from the inlet to the start of the built area. Finally, the top boundary is specified at a height of 5H. The domain is discretised into $175 \times 175 \times 40$ cells (stream-wise $\times$ span-wise $\times$ vertical). For the complex geometry two more simulations were conducted using $150 \times 150 \times 40$ and $225 \times 225 \times 60$ cells. Very little difference was observed in the velocity and turbulent kinetic energy field, implying grid independence, so that subsequent simulations for other geometries were conducted using the former resolution ($175 \times 175 \times 40$).

For the inlet boundary condition on the left side of the domain a standard logarithmic profile given by $U = u_* \ln(z/\dot{z}_o)/\kappa$ for the wind in the streamwise direction is used. A surface roughness value of $z_o = 0.3m$ and friction velocity $u_* = 0.06$ has been chosen; the latter to give a free stream velocity of 1 m/s. A turbulent kinetic profile is generated using the value of Uas $K = (0.01U^2)$, and for the eddy dissipation rate we use a profile given by $\varepsilon = \rho C_\mu K^2/\mu_t$ where ρ is the density

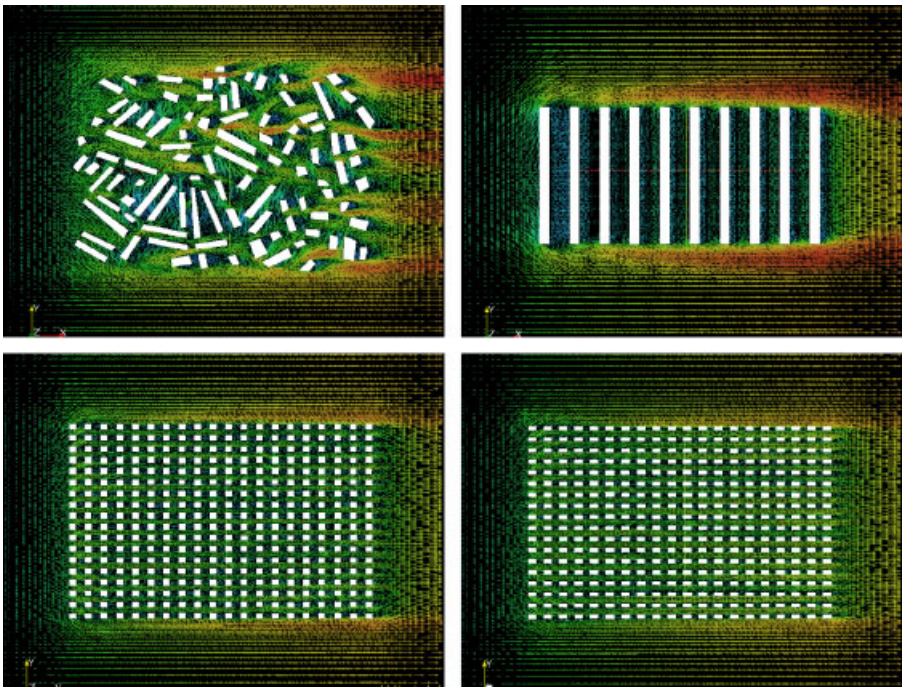

Figure 4. Velocity fields at 0.37H above the ground level for the four representations. This figure is available in colour online at wileyonlinelibrary.com/journal/joc

Table IV. Space averaged drag (F_x, F_y) and shear forces (S_x, S_y).

	F_x (N)	F_y (N)	S_x (N)	S_y (N)	$F_x + S_x$ (N)	$F_y + S_y$ (N)
Complex	8207	157	985	2.5	9194	160
Long canopies	14093	38.52	1424	1.95	15507	40.5
Simple cuboids 1	4931	−46	754	1.3	5658	−45
Simple cuboids 2	2911	−35	665	−3	3577	−38

of the air, $C_\mu = 0.09$ is a constant, and μ_t, the turbulent viscosity, is given by $\mu_t/\mu = 20$ where μ is the viscosity of air. An outlet boundary condition was applied on the right side. For the bottom side a wall boundary condition is specified, and for the rest of the domain surfaces a symmetry boundary condition was imposed.

The turbulence model used in this simulation is the standard $k - \varepsilon$ model. The advection scheme used for density and velocity is the HYBRID. A preconditioned (multi-grid) GMRES (Generalised Minimal Residual Method) solver is used for computing the pressure field. All CFD simulations were conducted for an isothermal (neutral atmosphere) stationary case. Convergence criteria of 10^{-5} for velocity and turbulent kinetic energy, and 10^{-4} for dissipation and continuity were imposed for all simulations.

3.3.2. CFD Results

In Figure 4, we present the velocity field for all four geometric representations at a height of 5.6 m (0.37H) above the ground plane. The more complex (real) representation is characterised by the formation of large vortices in the inter-building spaces. There is also a tendency for the flow to be deflected in the spanwise direction, due to the irregular orientation of the buildings. Long canopies strongly retard the flow, which tends to stagnate within the canopies. There is also an acceleration of flow at the ends of the long canopies. Within the other simplified representations, vortices are formed on the leeward side of the cuboids, which are small and well isolated from each other. Also, because these obstructions are non-continuous, the fluid motion remains essentially unidirectional in the streamwise sense. These observations (in Table IV) are also evident from the magnitude of the total drag and shear forces (obtained by integrating the pressure field over the building surface vectors) imposed by the buildings contained in the domain.

4. Concept of an equivalent city

With the advent of LIDAR technology, high-resolution data for buildings such as their shape, size, orientation, and location relative to other buildings and other urban morphological features are becoming more accessible. The National Urban Database and Access Portal Tool (NUDAPT) (Ching *et al.* 2009), for example, is a new

web-based urban data resource of the morphology and urban canopy parameters for American cities, which is based on LIDAR measurements. For a modern city like New York, these parameters are not difficult to derive as the cities are designed on grids. However, for a city like Basel, the canopy parameters are not so obvious. Equally important is that even if such simple morphological parameters were available (or indeed the raw data upon which they are based) for geometrically complex cities like Basel, they would not necessarily be compatible with the urban canopy model to be used, or indeed be a physically correct abstraction (in terms of radiation exchange and fluid dynamics) of the real complex geometry from which they are derived.

In the previous section, it was demonstrated that the same built volume can be redistributed in different ways to give different types of simplified representations. These different representations had very different drag and radiation absorption characteristics compared to the real geometries. It is thus important to identify an arrangement of a simplified geometry (as used in urban canopy models) for which these two quantities (drag and shortwave radiation absorption) will be roughly equivalent to those experienced by the corresponding real geometry. For this purpose, we introduce a new technique for fitting such an equivalent simplified geometry. In this, we define an equivalent geometry as 'the geometry which has the same built volume, horizontal, and vertical built area, offers the same drag and absorbs the same amount of shortwave radiation on vertical and horizontal surfaces as the complex/real representation.'

To find the equivalent geometry, a digitalised 3-D representation is sketched and parsed to the solver, which then identifies the corresponding equivalent geometry. The constraints here are that the total built surface area and volume of the two geometries should be equivalent. Mathematically,

$$S_{\text{complex}} = S_{\text{simplified}} \tag{4}$$

$$V_{\text{complex}} = V_{\text{simplified}} \tag{5}$$

Where S stands for vertical or horizontal built surface area and V stands for total built volume. This ensures that the building plan area fraction (λ_p) and wall area fraction (λ_w) do not change because of the mapping. This constraint is more important in those urban parameterisations where the atmospheric equations are modified for the built volume. The objective functions to be minimised are then defined by the following equations:

$$f_1 = Radiation^{\text{wall}}_{\text{complex}} - Radiation^{\text{wall}}_{\text{simplified}} \tag{6}$$

$$f_2 = Radiation^{\text{ground}}_{\text{complex}} - Radiation^{\text{ground}}_{\text{simplified}} \tag{7}$$

$$f_3 = Drag_{\text{complex}} - Drag_{\text{simplified}} \tag{8}$$

To demonstrate the methodology, we have chosen the three most obvious quantities: shortwave radiation incident on wall and ground surfaces, and total drag force experienced in the domain, but other parameters like the spatially averaged velocity or turbulent kinetic energy profiles could also be chosen.

4.1. Algorithm

The algorithm for finding the equivalent geometry can be enumerated as follows:

Step 1: 3-D geometry of the part of the city corresponding to a mesoscale tile is sketched and used as a complex representation. The geometry file is saved in the steriolithography (STL) format. If digital elevation models are available then they can be used instead.

Step 2: The STL files are converted into GTS (GNU Triangulated Surface) format using the open source GTS libraries (2010). The volume and surface area (both horizontal and vertical) of the buildings in the domain are computed. This representation is referred to as the complex representation.

Step 3: The diurnal shortwave radiation incident on different surfaces ($Radiation^{\text{wall}}_{\text{complex}}$, $Radiation^{\text{ground}}_{\text{complex}}$) and the total drag forces ($Drag_{\text{complex}}$) offered by the buildings in the domain are computed using the SRA and IST, respectively.

Step 4: Using the number of buildings sketched in Step 1, maximum and minimum permissible dimensions of buildings and streets found in the domain, and the total built volume and surface areas computed in Step 2, a simplified representation (in terms of B_1, B_2, W_1, W_2 and street width) of the urban area is constructed.

Step 5: For the simplified representation constructed in Step 4, a diurnal shortwave radiation profile incident on the different surfaces ($Radiation^{\text{wall}}_{\text{simplified}}$, $Radiation^{\text{ground}}_{\text{simplified}}$) and the total drag forces ($Drag_{\text{simplified}}$) are computed.

Step 6: The objective functions (f_1, f_2, f_3) are evaluated. If the functions are below the convergence criteria we have our equivalent simplified representation; else, Steps 4–6 are repeated.

It should be noted here that in the present work the choice of B_1, B_2, W_1, W_2 and street width is based on intuition and results from the previous iteration. For example, if we observe that the radiation incident on the walls in our simplified representation is considerably less than in its complex counterpart, then the parameters are adjusted in such a way as to increase the south-facing surfaces. Similarly, if the drag force is less in the streamwise direction, then the obstruction normal to the flow direction is increased.

4.2. Results

The algorithm explained in the last section was applied to the model of our chosen region of Basel. After several iterations, we identified a geometry which satisfies our definition of 'equivalent geometry' (Figure 5). We can see from Table V that the streamwise drag forces for both geometric models are comparable. Although the forces in the spanwise direction do differ, their magnitudes, compared to the streamwise forces, are negligible.

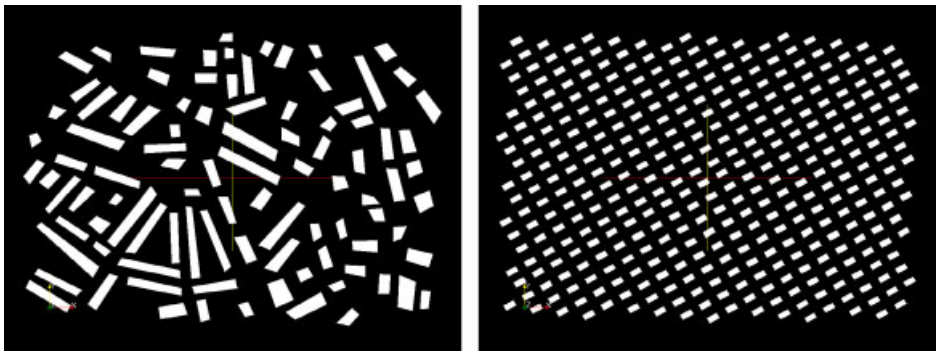

Figure 5. Complex geometry (left) and its equivalent form (right). This figure is available in colour online at wileyonlinelibrary.com/journal/joc

Furthermore, from Figure 6 we see that the profiles of radiation incident on the ground and wall surfaces for the complex and equivalent representations are now precisely superimposed. The radiation incident on the roof surfaces is not presented; it is proportional to the horizontal roof surface areas, which are identical for both representations. Each cube in the equivalent (simplified) representation has a dimension of 26.7 m × 15 m × 15 m. The West-East street width is 23.3 m and it is aligned at an angle of 30° to the east, while the South-North street width is 25 m and is aligned orthogonal to the other street. This simplified geometry, which is comprised of well defined urban canopy parameters obtained using a sound scientific basis, is fully compatible with the most popular Urban Canopy Models that are currently in use. We hope then that this new technique will help to generally improve the quality of urban climate predictions.

5. Conclusions

In this paper, the importance of the complexity of urban geometry on the spatially averaged quantities of incident shortwave irradiation and drag force has been studied. It was found that the error in the estimation of these quantities can be quite significant. We then introduced and tested a new algorithm for fitting an equivalent geometry (of the type used by urban canopy models) to any real complex geometry, based on minimising the error in drag force and incident shortwave radiation. This new method may be used to calibrate the geometric inputs to any urban canopy model in a rigorous way. It should be noted that in this work we have sketched the geometry of the complex city using Google Earth images, and then extruded each building to a standard height; an assumption which is reasonable for this location, based on field observations. However, the algorithm which is explained in this paper can handle non-uniformity in building height, so that with 3-D laser-scanned geometries becoming more and more accessible, one could, in principle, further improve upon the accuracy of our equivalent representation.

A potential shortfall of the methodology presented in this paper is that we suppose that drag and shortwave radiation are sufficient in themselves to judge the quality of fit between real and simplified geometries for urban climate prediction. This, of course, is not necessarily the case. We have focussed on these two for reasons of parsimony, but further work would be warranted to confirm, or otherwise, this hypothesis and in the latter case to select alternative or additional parameters. Finally, a process of manual trial and error has thus far been employed in fitting our simplified geometries by minimising differences in drag and radiation predictions. Subject to computational constraints the use of evolutionary algorithms would be more appropriate, enabling the available parameter space to be explored in a far more rigorous way. Work is under way to address both these issues.

Table V. Drag, shear and total force (in Newton).

-	F_x (N)	F_y (N)	S_x (N)	S_y (N)	$F_x + S_x$ (N)	$F_y + S_y$ (N)
Complex	8207	157	985	2.5	9194	160
Equivalent	7731	−346	894	5.8	8625	−340

6. Appendix A

A.1. Simplified radiosity algorithm

A.1.1. Governing equations

The Simplified Radiosity Algorithm (SRA) by Robinson and Stone (2004) is used to solve the shortwave radiation incident on the surfaces defining our urban scene. For some set of p sky patches, each of which subtends a solid angle Φ (Sr) and has radiance R ($\mathrm{Wm^{-2}Sr^{-1}}$) then, given the mean angle of incidence ζ (radians) between the patch and our receiving plane of slope β, together with the proportion of the patch that can be seen σ ($0 \leq \sigma \leq 1$), the direct sky irradiance ($\mathrm{Wm^{-2}}$) is given by

$$I_{d\beta} = \sum_{i=1}^{p} (R\Phi\sigma cos\zeta)_i \tag{9}$$

For this, the well known discretisation scheme due to Tregenza and Sharples (1993), is used to divide the sky vault into 145 patches of similar solid angle, and the Perez all-weather model (Perez, 1993) is used to calculate

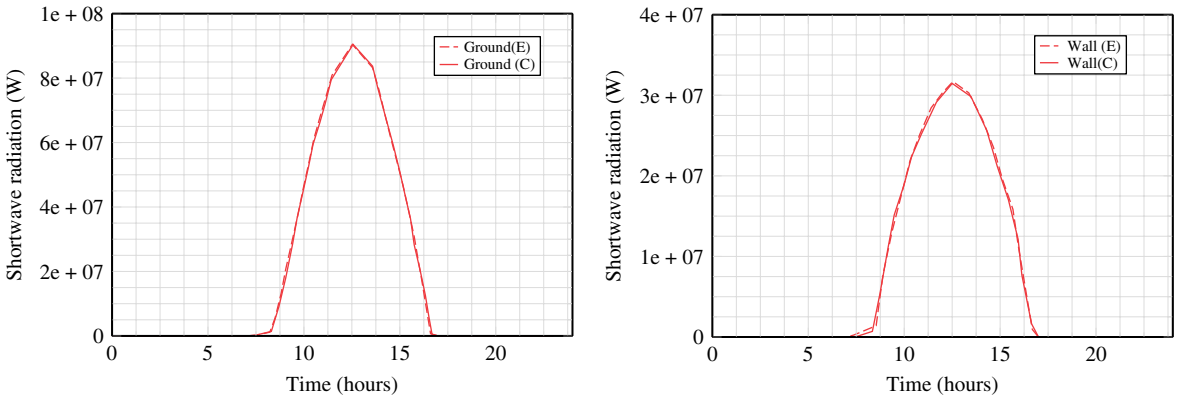

Figure 6. Hourly comparison of the amount of radiation incident on ground (left) and wall (right) surfaces. This figure is available in colour online at wileyonlinelibrary.com/journal/joc

the radiance at the centroid of each of these patches. The direct beam irradiance $I_{b\beta}$ is calculated from the beam normal irradiance I_{bn} which is incident at an angle ζ to our surface, of which some fraction ψ is visible from the sun, so that

$$I_{b\beta} = I_{bn}\psi cos\zeta \tag{10}$$

Now the direct sky and beam irradiance contributes to a given surface's radiance R, which in turn influences the irradiance incident at other surfaces visible to it, thus increasing their radiance, and vice versa. To solve this, a similar equation to that used for the sky contribution gives the reflected diffuse irradiance. In this case, two discretised vaults are used, one for above and one for below the horizontal plane, so that

$$I_{b\beta} = \sum_{i=1}^{2p} (R^* \Phi\omega \cos\xi)_i \tag{11}$$

where ω is the proportion of the patch which is obstructed by urban (reflecting) surfaces and R^* is the radiance of the surface which dominates the obstruction to this patch (in other words, that which contributes the most to ω). As noted earlier, R^* depends on reflected diffuse irradiance as well as on the direct sky and beam irradiances. For this, a set of simultaneous equations relating the beam and diffuse sky components to each surface's irradiance, which itself affects the reflected irradiance incident at other surfaces, may be formulated as a matrix and solved either iteratively or by matrix inversion (Robinson and Stone, 2004).

The principle complication in the above algorithm lies in determining the necessary view factors. For obstruction view factors, views encapsulating the hemisphere are rendered from each surface centroid, with every surface having a unique colour. Each pixel is then translated into angular coordinates to identify the corresponding patch as well as the angle of incidence. For sky view factors then, $\Phi\sigma\cos\zeta$ is treated as a single quantity obtained by numerical integration of $\cos\zeta.d\Phi$ across each sky patch. Likewise for $\Phi\omega\cos\zeta$, for which the dominant occluding surface is identified as that which provides the greatest contribution. A similar process is repeated for solar visibility fractions for each surface, for which a constant size scene is rendered from the sun position. For further details describing the implementation of this SRA the reader is referred to Robinson and Stone (2005).

A.1.2. Scene description and surface tesselisation

The urban scene is sketched using NURBS (Non Uniform Rational B-Spline) based on the solid modeling software, Rhinoceros. A 2-D projection of all the buildings is sketched using Google images as a rough guideline. A Boolean operation is then conducted to remove the projections from the floor of the domain to obtain the ground surface. The 2-D building projections are then vertically extruded to the appropriate height and all the surfaces including the ground surfaces are discretised into small triangles. The resulting geometry file is then exported in STL file format, which is converted to a format compatible with the SRA program.

To sum up, computation of radiation using the SRA involves the following steps: (1) Geometrical description of the scene (urban geometry and ground) and surface tesselisation; (2) Division of sky vaults into 145 patches and computation of radiance at the centroid of these patches; (3) Computation of sky patch/occlusion/sun view factors; and (4) Solving the matrices to obtain the shortwave radiation at each time step.

A.1.3. Validation results

Figure 7 shows a comparison of annual shortwave radiation computed by the backward ray tracing program RADIANCE (top left) and the SRA (top right). Figure 7 (bottom) shows the difference between the values computed by the two models. From this we conclude that the SRA computes the incident irradiation within acceptable limits for our applications. Further details concerning the validation of the SRA can be found in Robinson and Stone (2004, 2005)

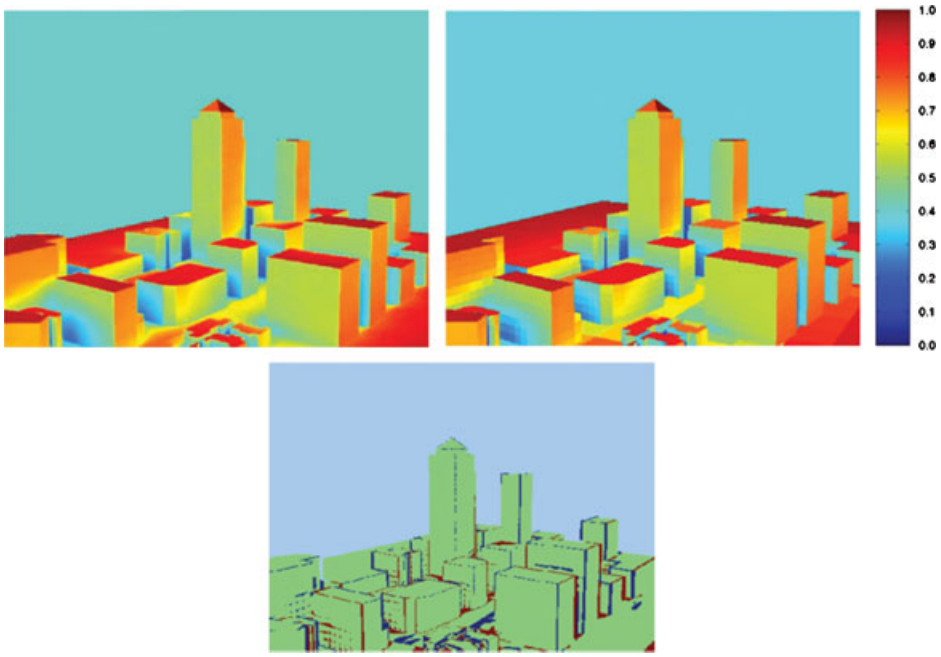

Figure 7. Prediction of annual solar radiation (in MWh) throughout a simplified 3-D model of Canary Wharf in London, UK RADIANCE (left) and SRA (right) based on surfaces. Below: Difference between the two models (green corresponds to a difference of below 10%). This figure is available in colour online at wileyonlinelibrary.com/journal/joc

7. Appendix B

B.1. Immersed surface technique

The term 'Immersed Surface Technique (IST)' was first used in reference to a method developed by Peskin (1977) to simulate cardiac mechanics and associated blood flow. The distinguishing feature of this method was that the whole simulation was carried out on a Cartisean grid which did not conform to the geometry of the heart. A novel procedure was formulated for imposing the effects of the immersed boundary on the flow, rather than fitting a more complex mesh to the bounding surfaces. The IST used in this work is a variant of this method (TransAT, 2010). In this method, solid walls are represented by a Level Set function representing the exact distance to the surface. This takes a value of zero at the surface and is positive in the fluid and negative in the solid. Both the liquid and solid have different thermophysical properties based on this Level Set function. In practice, a computer aided design (CAD) file is immersed in a cubical grid covered by a Cartesian mesh. The Navier-Stokes equations are modified to account for the presence of the solid Level Set function. The treatment of viscous shear at the solid surface is handled in very much the same was as in conventional computational fluid dynamics (CFD) codes. This is explained with the help of equations in the following subsection.

B.1.1. Governing equations

The immersed surface is represented on the fluid grid by a Level Set function (ϕ_s), where $\phi_s = 0$ represents the fluid–solid interface. The flow equations in the solid and fluid domain are combined using a smooth Heaviside function $H(\phi_s)$ which has value 1 in the fluid phase and 0 in the solid phase.

$$H(\phi_s) = \frac{1}{2}\left(1 - \tanh\left(\frac{2\phi_s}{\delta_{sf}}\right)\right) \tag{12}$$

where, δ_{sf} is the solid–fluid finite interface thickness.

The following mass and momentum equations are used for the solid phase:

$$\frac{\partial \rho^s}{\partial t} + \frac{\partial}{\partial x_i}(\rho^s u_i^s) = 0 \tag{13}$$

$$\frac{\partial \rho^s u_i^s}{\partial t} + \frac{\partial}{\partial x_j}(\rho^s u_i^s u_j^s) = 0 \tag{14}$$

For the case of non-moving immersed surfaces, the solid phase velocity is set to zero ($u_i^s = 0$). The standard Navier-Stokes equations are used for the fluid phase.

$$\frac{\partial \rho^f}{\partial t} + \frac{\partial}{\partial x_i}(\rho^f u_i^f) = 0 \tag{15}$$

$$\frac{\partial \rho^f u_i^f}{\partial t} + \frac{\partial}{\partial x_j}(\rho^f u_i^f u_j^f) = -\frac{\partial p^f}{\partial x_i} + \frac{\partial}{\partial x_j}\left(2\mu^f \frac{\partial S_{ij}^f}{\partial x_j}\right) + \rho^f g_i \tag{16}$$

Combining the solid and fluid equations into a single equation by multiplying the phase equations by the

respective Heaviside functions and summing up, we obtain the following equations:

$$\frac{\partial \rho}{\partial t} + \frac{\partial}{\partial x_i}(\rho u_i) = 0 \tag{17}$$

$$\frac{\partial \rho u_i}{\partial t} + \frac{\partial}{\partial x_j}(\rho u_i u_j) = -H(\phi_s)\frac{\partial p^f}{\partial x_i} + \frac{\partial}{\partial x_j}\left(2\mu \frac{\partial S_{ij}}{\partial x_j}\right) + H(\phi_s)\rho^f g_i - 2\mu^f S_{ij}^f n_j \delta(\phi_s) \tag{18}$$

where, the composite quantities ρ and u_i are defined as

$$\rho = H(\phi_s)\rho^f + (1 - H(\phi_s))\rho^s \tag{19}$$

$$\rho u_i = H(\phi_s)\rho^f u_i^f + (1 - H(\phi_s))\rho^s u_i^s \tag{20}$$

The last term in the RHS of Equation 13 is a viscous shear stress at the wall, where n_j is the normal to the fluid–solid interface, and $\delta(\phi_s)$ is the Dirac delta function representing the location of the interface. The wall shear stress itself is modeled as (Beckermann *et al*., 1999)

$$2\mu^f S_{ij}^f n_j = 2\mu^f \left(\frac{\rho}{\rho^f}\right) u_i \delta(\phi_s) \tag{21}$$

When used in combination with RANS (Reynolds Averaged Navier Stokes) turbulence modeling with wall functions, the wall shear is calculated using the logarithmic law of the wall.

B.1.2. IST in an urban context

Construction of city geometry with a 3-D modeling tool is trivial and can be reasonably quick depending on the availability of existing data. Such geometries can be quickly converted into an STL CAD file. The use of a Cartesian mesh when using the IST technique also cuts down the grid generation time and reduces memory requirements, so that the real simulation time is also reduced; particularly as very efficient algorithms are available for simulating fluid flow using a Cartesian mesh. Thus, this IST technique makes it possible to simulate larger (urban scale) domains, relative to a conventional CFD approach.

B.1.3. Validation: flow over cube

By way of validation we use a test setup consisting of a cube of height H contained within a channel, as shown in Figure 8. The Reynolds number is $\mathrm{Re} = U_b H/\nu = 40000$, based on the incoming mean bulk velocity, U_b, and the obstacle height H. Even though the geometry of the flow configuration is rather simple, the flow is physically quite complex, with multiple separation regions and vortices. Martinuzzi and Tropea (1993) carried out flow visualisation studies and detailed Laser Doppler Anemometry (LDA) measurements of the fluid flow through this configuration from which the mean velocity components and the various Reynolds stresses are available. The oncoming turbulence intensity at roof height is relatively low ($T_u = u'^2/U_b \approx 0.03$). The present simulation setup is borrowed from Lakehal and

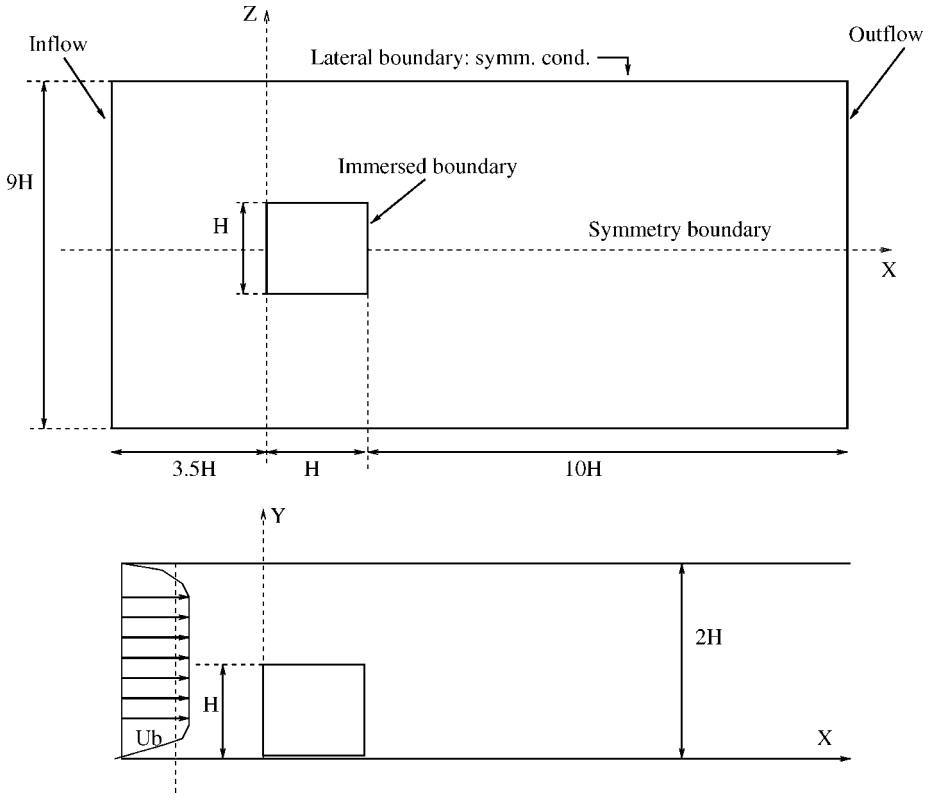

Figure 8. IST simulation: Set up to simulate flow over a cube.

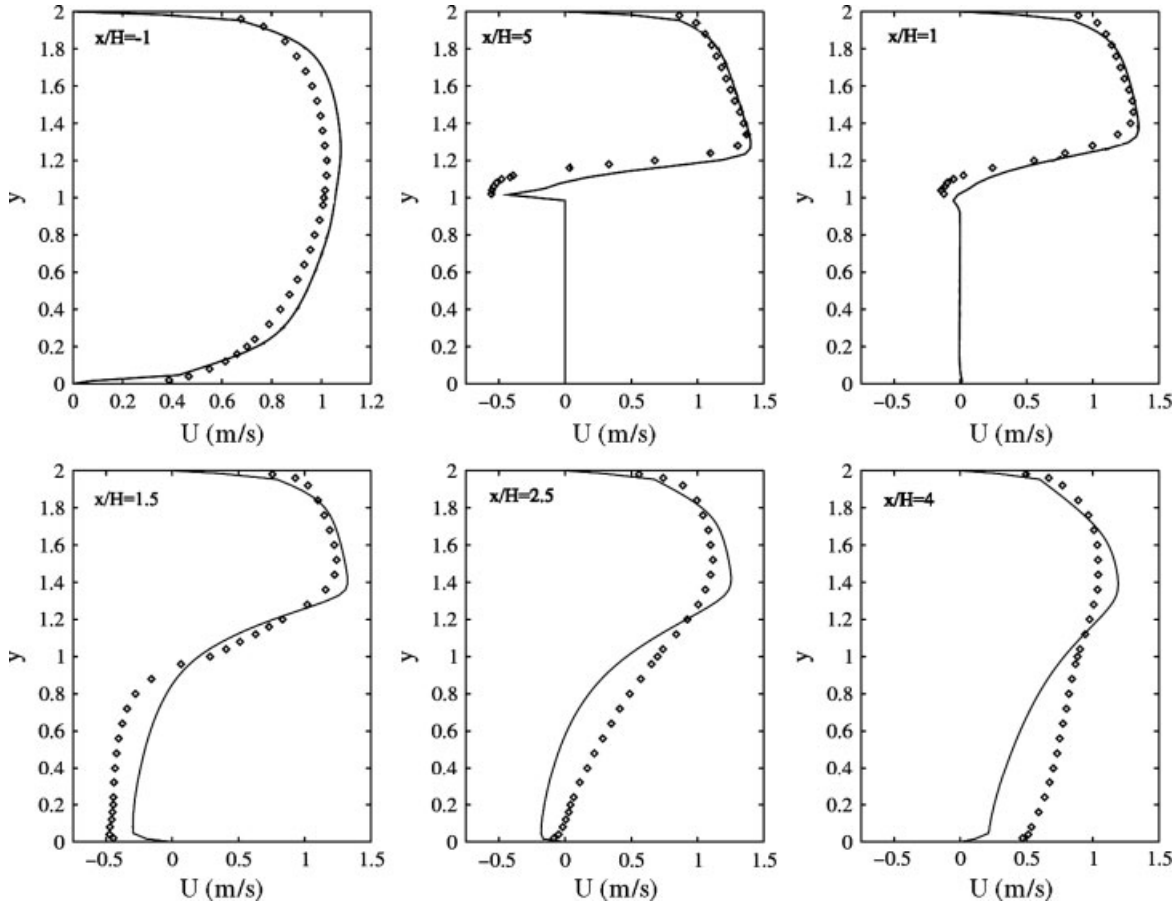

Figure 9. IST (solid line) vs experimental data (diamond symbol) at different x/H locations in the domain.

Rodi (1997) and Breuer *et al*. (1996). Earlier calculations of these authors using various grids (with the traditional block-defined meshing) employed a $110 \times 32 \times 32$ grid for the standard $k-\varepsilon$ model using wall functions, with the width of the near-wall cell set to correspond to $10 < y^+ < 25$, where y^+ is the non-dimensional wall distance defined as $y^+ = u_* y/\upsilon$ (u_* is the friction velocity, y is the distance from the wall and υ is kinematic viscosity). A similar grid was used for the new computations, but this time using IST. A comparison of results from the IST simulations with the measurements of Martinuzzi and Tropea (1993) is presented in Figure 9, in terms of the streamwise velocity components at different values of x/H (-1.0, 0.5, 1, 1.5, 2.5 and 4) at the symmetry plane. All U-velocity profiles agree well with the measurements at $x/H = -1.0$ upstream of the cube. However, differences between the CFD results and the experiment are apparent at the middle of the cube ($x/H = 0.5$), as well as at the back face of the cube ($x/H = 1.0$). At $x/H = 1.5$, the profiles predicted by the model agree fairly well with the experiments in the region above the roof height. Below this, the reverse flow velocity is under-predicted. Further explanations of the flow characteristics can be found in Lakehal and Rodi (1997). From the present qualitative comparison we can simply conclude that IST predictions are in reasonable agreement with experimental observations.

References

Beckermann C, Diepers H-J, Steinbach I, Karma A, Tong X. 1999. Modeling melt convection in phase-field simulations of solidification. *Journal of Computational Physics* **154**: 468–496.

Breuer M, Lakehal D, Rodi W. 1996. Flow around a surface mounted cubical obstacle: Comparison of LES and RANS-Results. *Notes of Numerical Fluid Mechanics*. Vieweg Verlag: Braunschweig **53**: 22–30.

Britter RE, Hanna SR. 2003. Flow and dispersion in urban areas. *Annual Review of Fluid Mechanics* **35**: 469–496.

Ching J, Brown M, Burian S, Chen F, Cionco R, Hanna A, Hultgren T, McPherson T, Sailor D, Taha H, Williams D. 2009. National urban database and access portal tool, NUDAPT. *Bulletin of the American Meteorological Society* **90**(8): 1157–1168.

GTS library. http://gts.sourceforge.net. [accessed September 25 2010].

Harmann IN, Best MJ, Belcher SE. 2004. Radiative Exchange in an Urban Street Canyon. *Boundary-Layer Meteorology* **110**: 301–316.

Kondo H, Liu FH. 1998. A study of the urban thermal environment obtained through one-dimensional urban canopy model. *Journal of Japan Society for Atmospheric Environment* **33**: 179–192.

Kusaka H, Kondo H, Kikegawa Y, Kimura F. 2001. A simple single-layer urban canopy model for atmospheric models: Comparison with multilayer and slab models. *Boundary Layer Meteorology* **101**: 329–358.

Lakehal D, Rodi W. 1997. Calculation of flow past a surface-mounted cube with 2-layer models. *Journal of Wind Engineering and Industrial Aerodynamics* **67**: 65–78.

Martilli A, Clappier A, Rotach M. 2002. An urban surface exchange parameterization for mesoscale models. *Boundary Layer Meteorology* **104**: 261–304.

Martinuzzi R, Tropea C. 1993. The flow around surface-mounted, prismatic obstacles placed in a fully developed channel flow. *Journal of Fluid Engineering* **115**: 85–91.

Masson V. 2000. A physically-based scheme for the urban energy budget in atmospheric models. *Boundary Layer Meteorology* **94**: 357–397.

Mills G. 1997. An urban canopy-layer climate model. *Theoretical and Applied Climatology* **57**: 229–244.
Noihan J. 1981. A model for the net total radiation flux at the surfaces of a building. *Building and Environment* **16**: 259–266.
Perez RRS, Michalsky J. 1993. All-weather model for sky luminance distribution-preliminary configuration and validation. *Solar Energy* **50**(3): 235–245.
Peskin C. 1977. Numerical analysis of blood flow in the heart. *Journal of Computational Physics* **25**: 220–238.
Robinson D, Stone A. 2004. Solar radiation modeling in the urban context. *Solar Energy* **77**: 295–309.
Robinson D, Stone A. 2005. A simplified radiosity algorithm for general urban radiation exchange. *Building Services Engineering Research and Technology* **26**: 271–284.
Rotach M. 2001. Urban scale-dispersion modelling using a Lagrangian particle dispersion model. *Boundary Layer Meteorology* **99**: 379–410.
Roth M. 2000. Review of atmospheric turbulence over cities. *Quarterly Journal of Royal Meteorological Society* **126**: 941–990.
Salamanca F, Krpo A, Martilli A, Clappier A. 2009. A new building energy model coupled with an urban canopy parameterization for urban climate simulation – part I: formulation, verification and sensitivity analysis of the model. *Theretical and Applied Climatology* **99**: 331–344.
Swaid H. 1993. The role of radiative/convective interaction in creating the microclimate of urban street canyons, boundary layer meteorology **64**: 231–259.
TransAT. Transport Phenomena Analysis Tool. Website: http://ascomp.ch/. [accessed March 07 2010].
Tregenza P, Sharples S. 1993. *Daylighting Algorithms*, ETSUS: UK, 1350–1993.
Vu TC, Asaeda T, Ashie Y. 1999. Development of a numerical model for the evaluation of the urban thermal environment. *Journal of Wind Engineering* **81**: 181–196.

